EARTHQUAKE ENGINEERING AND STRUCTURAL DYNAMICS
Earthquake Engng Struct. Dyn. (2017)
Published online XX in Wiley InterScience-(www.interscience.wiley.com). DOI: XX

Seismic Intensity Measures for Above-Ground Liquid Storage Tanks

Konstantinos Bakalis [1,*,†] , Mohsen Kohrangi[2] and Dimitrios Vamvatsikos[1]

[1] *School of Civil Engineering, Institute of Steel Structures, National Technical University of Athens, Greece*
[2] *University School of Advanced Studies IUSS Pavia, Pavia, Italy*

SUMMARY

A series of scalar and vector intensity measures is examined to determine their suitability within the seismic risk assessment of liquid storage tanks. Using a surrogate modelling approach on a squat tank that is examined both under anchored and unanchored support conditions, incremental dynamic analysis is adopted to generate the distributions of response parameters conditioned on each of the candidate intensity measures. Efficiency and sufficiency metrics are employed in order to perform the intensity measure evaluation for individual failure modes, while a comparison in terms of mean annual frequency of exceedance is carried out with respect to a damage state that is mutually governed by the impulsive and convective modes of the tank. The results reveal combinations of spectral acceleration ordinates as adequate predictors, among which the average spectral acceleration is singled out as the optimal solution. The sole exception is found for the sloshing-controlled modes of failure, where mainly the convective-period spectral acceleration is deemed adequate to represent the associated response due to their underlying linear relationship. A computationally efficient method in terms of site hazard analysis is finally proposed to serve in place of the vector-valued intensity measures, providing a good match for the unanchored tank considered and a more conservative one for the corresponding anchored system.

KEY WORDS: performance-based earthquake engineering; incremental dynamic analysis; intensity measures; uncertainty; demand; capacity;

1. INTRODUCTION

Liquid storage tanks comprise a vital link between the exploration/exploitation of petrochemical energy resources and the distribution of their products to the public. To ensure the structural integrity of such important structures against the (potentially) devastating socioeconomic impact of a major earthquake, state-of-the-art techniques should be employed [1]. Previous earthquake events (e.g. Alaska 1964 [2], Izmit 1999 [3], Tohoku 2011 [4]) have revealed several levels of damage on tanks, spanning from easy-to-repair structural damage to

* Correspondence to: Konstantinos Bakalis, National Technical University of Athens, 9 Iroon Polytechneiou, Athens 15780, Greece.
† E-mail: kbakalis@mail.ntua.gr

complete loss of the stored material, often associated with one or more modes of failure. Although they might relate to varying degrees of repair actions, these failure modes form a union of events that govern the violation of a specific system (global) damage state (*DS*) [5,6]. In the course of seismic performance assessment, capturing the aforementioned failure modes requires employing appropriate engineering demand parameters (*EDPs*, e.g. stress, strain) [7], the pertinent thresholds [7], a suitable structural model [8] and multiple ground motion records, characterised by pertinent intensity measures (*IMs*) such as the peak ground acceleration (*PGA*) and the first-mode spectral acceleration $S_a(T_1)$ [9,10].

The information provided above may be efficiently blended into the Performance-Based Earthquake Engineering (PBEE) concept, originally developed by Cornell and Krawinkler [1] for the Pacific Earthquake Engineering Research (PEER) Centre, whereby the end-product is typically given in terms of the mean annual frequency (MAF) 'λ' of exceeding e.g. monetary loss or downtime thresholds. Nevertheless, the seismic assessment is often conveniently performed using the intermediate product of MAF of exceeding *DS* thresholds [10,11], by integrating the associated *IM*-conditional probability that demand (*D*) exceeds capacity (*C*) with the annual rate of exceeding *IM* values as:

$$\lambda(DS) = \int_{IM} \mathrm{P}(D > C \mid IM)\, \left|\mathrm{d}\lambda(IM)\right|. \tag{1}$$

In Equation (1), P(D>C|IM) is referred to as the 'fragility function', while dλ(IM) is the differential of the seismic hazard curve for the *IM* of interest, which is commonly obtained using a probabilistic seismic hazard analysis (PSHA) [12]. Regardless of whether one seeks the MAF of a *DS* or level of loss, the sole parameter that always remains present is the hazard curve, which provides information on the rates of exceeding certain levels of seismic intensity in terms of MAF. Evidently, the *IM* becomes a key element for every assessment-related study, serving as an interface variable among the various parameters that affect 'λ'.

Adopting an *IM* to perform the seismic risk evaluation on a liquid storage tank is not straightforward and the reason mainly lies in the complex response that these structural systems tend to develop during earthquakes. Under ground motion excitation, the contained fluid is essentially divided into two modal masses that are typically considered decoupled [8,13] (Figure 1A). The translational response is then dominated by a short-period (e.g. T_i=0.1-0.3s) mode of vibration, also known as the (rigid-) impulsive component, and is highly associated with modes of failure such as buckling, plastic rotation and anchor-bolt failure. On the other hand, the remaining portion of the contained fluid is excited at (ultra) long-period modes of vibration (e.g. T_c=4.0-7.0s), refers to the sloshing of the free fluid-surface, and is tied to roof and upper-course damage on the tank. This so-called convective component seldom contributes noteworthy overturning actions on the tank and thus the decoupling among impulsive and convective may reasonably be taken for granted especially for squat tanks [14,15]. Evidently, from an assessment point of view, it appears that one is left with a single system influenced by two (largely uncorrelated) spectral acceleration ordinates [e.g. $S_a(T_i)$ and $S_a(T_c)$], and little information available on the existing literature regarding the *IM* that better suits this particular case [16,17]. The aim of this study is to explore the choice of the *IM* for liquid storage tanks based on quantitative metrics, and come up with the 'optimal' solution from a pool of candidate *IMs*, ranging from simple to complicated ones.

2. SCALAR OR VECTOR?

A suitable *IM* should not only serve as an index of the ground shaking severity, but also as a

DOI: XX

good predictor of the *EDPs* of interest in the structure. In general, the choice of the intensity measure is important and the first reason is variability. Reducing variability implies that a smaller number of records is required to achieve the same level of confidence on the numerical output [18]. This is the well-known requirement of *efficiency* according to Luco and Cornell [19]. The second reason is *sufficiency*, which states that the *IM* should render the structural response independent of other seismological or ground motion characteristics [e.g. magnitude (M_w), distance, pulse duration, epsilon (ε)], thus removing the bias introduced when this dependence is ignored in Equation (1). Obviously, any sort of discussion around efficiency, sufficiency and bias makes sense so long as the hazard curves of the intensity measure under investigation can actually be computed [20,21]. Further desirable properties have been proposed for *IMs* [21], but in the opinion of the authors they can be folded back to the above two fundamental ones without loss of generality.

2.1. Scalar Intensity Measures

Traditionally, the intensity measure is a scalar variable represented by well-known spectral quantities, such as *PGA* and $S_a(T_1)$. As much as the aforementioned *IMs* may seem useful for the assessment of certain structural systems (e.g. low and/or mid-rise frame-structures respectively), their suitability cannot be taken for granted for the entire range of civil engineering structures. The reason is that individual spectra carry too much variability that cannot always be captured by $S_a(T_1)$ or *PGA* alone; in fact, there are several cases in recent literature where alternative scalar *IMs* or even complex combinations of them are adopted to adequately represent the seismic input on a given structural system [18,22]. For instance, the first-mode inelastic spectral displacement and its combination with higher mode spectral ordinates have been proposed for pulse-like and non-pulse-like ground motions [23,24], while the geometric mean of the $S_a(T_1)$ values along the longitudinal and transverse directions of a three-dimensional (3D) moment resisting frame is considered [25] in place of the arbitrary $S_a(T_1)$ ground motion component, especially for cases that the fundamental period of the structure does not predominately favour either of the building axes.

Along these lines, research efforts have resulted in the generation of seismic intensity measures that often consider the product of multiple spectral acceleration ordinates. Such *IMs* normally involve $S_a(T_1)$ along with a modification factor that accounts for spectral shape. This was initially proposed by Cordova et al. [26] incorporating the geometric mean of $S_a(T_1)$ and $S_a(2T_1)$, attempting to capture the apparent 'elongation' of the fundamental period due to structural damage, and was further studied by Vamvatsikos and Cornell [18] who added higher mode periods. This idea has evolved into the average spectral acceleration ($AvgS_a$) whereby one employs n spectral ordinates at equally-spaced multiple periods T_{Rj} within a range [T_L, T_H] that includes T_1 and is defined by a lower (T_L) and higher (T_H) bound:

$$AvgS_a = \left[\prod_{j=1}^{n} S_a\left(T_{Rj}\right)\right]^{1/n}. \tag{2}$$

Studies by many researchers have shown that a wide variety of *IMs* defined according to the general frame of Equation (2) can offer substantial efficiency and sufficiency for building structures [22,27–32].

2.2. Vector-valued Intensity Measures

Despite the amount of work performed to date, it seems that most scalar *IMs* are always going

DOI: XX

to suffer from some level of insufficiency, particularly when the *EDP*|*IM* relationship strongly depends on additional ground motion parameters. In view of further improving the accuracy with respect to the MAF estimation, the concept of vector-valued intensity measures has emerged, offering the ability to better tackle sufficiency and efficiency. There are several examples where vector-valued IMs may be desirable, such as the case of incorporating higher or "elongated" modes of buildings, or even that of buried pipelines subject to 3D deformation at fault crossings [18,22,33–35].

In spite of the potential for higher fidelity, the use of vector-valued *IMs* increases the complexity of application by requiring the ability to conduct vector-valued probabilistic seismic hazard analysis (VPSHA) [33]. Another issue is the analysis effort that is carried out to determine the *EDP*|*IM* relationship [36] and thus the multi-dimensional fragility surface [37]. This is the well-known 'curse of dimensionality' whereby increasing the dimensions of the *IM* necessitates even more samples for reliable estimation of the fragility. For practical purposes, these complexities have naturally decelerated the use of vector-valued *IMs*, which are currently confined within the academic environment, mainly aiming towards the validation and quantification of the accuracy of scalar ones.

3. MODELLING, DAMAGE STATES AND EDPS

The surrogate modelling approach proposed by Bakalis et al. [8] (Figure 1B), is adopted to carry out the nonlinear dynamic analyses required for this study. The so-called "Joystick" model follows the general formulation and associated assumptions offered by Malhotra and Veletsos [38]; it consists of radially spaced rigid beams, that essentially form the base plate of the tank, and are supported by vertically-oriented elastic multilinear springs. The tensile and compressive properties of those edge-springs are assigned the uplift resistance of a $2R_t$ long (where R_t is the radius of tank), uniformly loaded (due to hydrostatic loading) beam (strip) model, as explicitly shown in Figure 1C [6,8]. The base plate is connected to an elastic element that carries the impulsive mass of the tank, and is assigned properties such that the fundamental period of the entire system equals the prediction offered by Malhotra [13,39]. This model is able to simulate (either directly or indirectly) commonly observed modes of failure such as shell buckling, base plate plastic rotation, uplift and anchor bolt deformation (where anchorage is necessary to supply the system with additional stability on top of self-weight anchoring [40]). Sloshing response is not explicitly modelled; instead, taking advantage of the decoupling among the impulsive and convective modes of vibration [38,41–43], it is taken into account through the Eurocode 8 [13,39] equation (A.15) that presents a linear relationship between the sloshing wave height (d) and the elastic convective period spectral acceleration for an appropriately defined fluid damping κ_f:

$$d = 0.84 R_t S_a\left(T_c, \kappa_f\right)/g \,. \tag{3}$$

To facilitate the application of the PBEE concept, the aforementioned failure modes are combined to form system damage states of increasing severity for both anchored and unanchored liquid storage tanks [5,6]. For instance, minor damage on the roof and/or upper course of the tank due to sloshing of the contained fluid, as well as yielding of the foundation anchor bolts, may be characterised as slight structural damage (i.e. *DS*1). Moderate plastic rotations (i.e. order of 0.2rad) on the base-plate, significant roof damage, and fracture of the foundation anchor bolts may be deemed as severe structural damage without leakage of the stored material (i.e. *DS*2). Similarly, the leakage potential (i.e. *DS*3) may be triggered either

DOI: XX

due to an elastic-plastic buckling failure known as the elephant's foot buckling (EFB), or extreme base-plate plastic rotations (i.e. order of 0.4rad). Table 1 summarises the *DS* classification for liquid storage tanks, with respect to the system support conditions (i.e. anchored versus unanchored). As discussed above, the violation of each *DS* is triggered when an *EDP* value—i.e. d for sloshing wave height obtained from equation (3), δ for anchor bolt deformation obtained from the "Joystick" edge-springs response, θ_{pl} for base plate plastic rotation obtained either from direct model measurements or via the Eurocode 8 relationship (A.61), and σ_m for tank wall meridional stress obtained by converting the "Joystick" edge-spring vertical force to stress [6]—exceeds the prescribed *EDP* capacity: the available freeboard d_f for sloshing, the anchor bolt yield δ_y and fracture δ_u deformation (e.g. δ_u=100mm [8]), the 0.2rad and 0.4rad limits for base plate plastic rotation, and the σ_{EFB} limit for EFB [6,39]. The simultaneous effect of both impulsive and convective-controlled *EDPs* on certain damage states

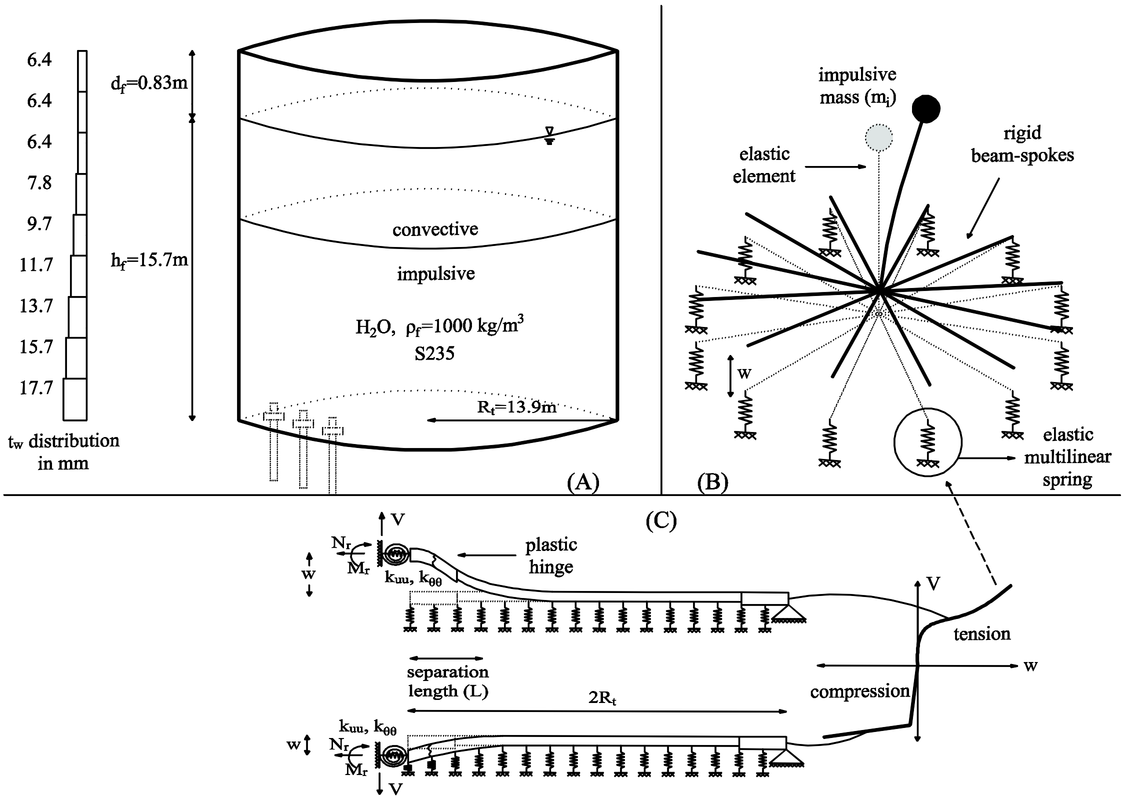

Figure 1: A, Impulsive versus convective fluid component, and properties of the case study liquid storage tank. Depending on the presence of anchors, the system is either anchored or unanchored. B, The "Joystick" surrogate model [6,8] and its deflected shape. The rigid base, initially resting on the edge springs, is shown uplifting by rotating around the ground contact point(s) following the displacement of the impulsive mass that represents the fluid. C, The strip model of the tank base plate, as employed to derive the force-deformation relationship of the edge springs.

Table 1: Damage state classification for anchored and unanchored liquid storage tanks.

System Support Conditions	Damage States	Damage State Violation
	*DS*1	d>1.0×d_f or δ>δ_y
Anchored	*DS*2	d>1.4×d_f or θ_{pl}>0.2rad or δ>δ_u
	*DS*3	σ_m>σ_{EFB} or θ_{pl}>0.4rad
	*DS*1	d>1.0×d_f
Unanchored	*DS*2	d>1.4×d_f or θ_{pl}>0.2rad
	*DS*3	σ_m>σ_{EFB} or θ_{pl}>0.4rad

DOI: XX

(e.g. $DS1$ for anchored tanks only and $DS2$ for both anchored and unanchored) constitutes the applicability of conventional IMs (e.g. PGA) questionable for the seismic risk assessment of liquid storage tanks, as extensively discussed in the following.

4. IM SELECTION

Several candidate IMs (Table 2) are selected to investigate their suitability within the seismic risk assessment of liquid storage tanks. Besides the obvious choice of $S_a(T_i)$, the relatively short fundamental period of tanks (i.e. T_i=0.1-0.3s) allows also considering PGA. Another obvious choice is that of $S_a(T_c)$, which by default is going to be the perfect predictor for the sloshing-related modes of failure (due to their inherently linear relationship assumed for the 'Joystick' model [13,39]), and a rather poor one for the rest of $EDPs$ and failure modes. Attempting to bridge the wide gap between the impulsive and convective periods, the geometric mean of various spectral quantities is considered. Combinations of $S_a(T_i)$ with $S_a(T_c)$, $S_a(T_i)$ with spectral accelerations at elongated impulsive periods of vibration (i.e. $1.5T_i$), PGA with $S_a(T_c)$, as well as the (scalar) state-of-the-art $AvgS_a$ for various ranges of period (i.e. 0.1s-0.6s, 0.1s-1.0s and 0.1s-1.5s) are taken into account. It should be noted that behind the choice of such high period upper bounds for the $AvgS_a$, lies in the nonlinear-elastic nature of the "Joystick" model, which forces the system to remain on the low-stiffness hardening branch during loading/unloading and reloading, in contrast to the elastic segments of unloading/reloading of an elastic-hardening system. In general, the concept of combined S_a values may also be deemed a strong candidate IM for the seismic risk evaluation of a group of tanks with varying geometry (and thus T_i and

Table 2: Candidate IMs for the seismic risk assessment of a liquid storage tank with T_i=0.22s and T_c=5.6s.

Intensity Measures*		Abbreviation
Scalar		
PGA		IM_{s1}
$S_a(T_i)$		IM_{s2}
$S_a(T_c)$		IM_{s3}
$\sqrt{S_a(T_i)\cdot S_a(T_c)}$		IM_{s4}
$\sqrt{S_a(T_i)\cdot S_a(1.5T_i)}$		IM_{s5}
$\sqrt{PGA\cdot S_a(T_c)}$		IM_{s6}
$AvgS_a=\left[\prod_{j=1}^{n} S_a(T_{Rj})\right]^{1/n}$	$0.1s \le T_{Rj} \le 0.6s$ ($\approx 2.7T_i$)	$IM_{s7\text{-}1}$
	$0.1s \le T_{Rj} \le 1.0s$ ($\approx 4.5T_i$)	$IM_{s7\text{-}2}$
	$0.1s \le T_{Rj} \le 1.5s$ ($\approx 6.8T_i$)	$IM_{s7\text{-}3}$
Vector		
$\{PGA, S_a(T_c)\}$, or equivalently $\{PGA, S_a(T_c)/PGA\}$		IM_{v1}
$\{S_a(T_i), S_a(T_c)\}$, or equivalently $\{S_a(T_i), S_a(T_c)/S_a(T_i)\}$		IM_{v2}

*All spectral ordinates refer to the geometric mean of the longitudinal and transverse earthquake recordings

T_c) [22,28,29]. This is an interesting problem that requires thorough investigation and is

DOI: XX

expected to be covered in a future direction of our research. Finally, the vectors of {PGA, $S_a(T_c)$} and {$S_a(T_i)$, $S_a(T_c)$} are considered as a potentially more accurate way of incorporating the effect of T_c without compromising that of T_i as done in a scalar combination. Note that, without loss of generality, the second element of the above vectors may be replaced by its ratio over the first, as indicated in Table 2; this transformation will be used to better distinguish the effect of each vector component having the first element being scalable and the second constant for any given record [18].

5. SEISMIC HAZARD AND RECORD SELECTION

A site of major oil refineries in Elefsina, Greece with coordinates of (23.507°N, 38.04°E) is adopted to perform all PSHA and VPSHA-related computations, the results of which are summarised in Figure 2 for both the scalar and vector *IMs* examined. OpenQuake [44], open-source software for seismic hazard and risk assessment developed by the Global Earthquake Model Foundation is used to perform the seismic hazard and disaggregation computations of this study. PSHA and VPSHA are based on the SHARE Project [45] area source model and the ground motion prediction equation (GMPE) proposed by Boore and Atkinson [46] is used for all purposes of this study. It should be noted that VPSHA computations are based on the *indirect* approach [47].

The structural response is significantly dependent on the seismicity of the site where the structure is located. Record selection provides the link between the site hazard and the structural response, therefore, it is important for the ground motion set used for response history analysis to be compatible with the seismicity at the site. Herein, two approaches are employed for selection of the records to use in response history analysis. Initially, a set of 135 "ordinary" ground motion record pairs (i.e. non-pulse-like, non-long-duration) obtained from the PEER-NGA database [48] is adopted, hereafter referred to as GMset-plain. Note that this record set is 'not' used for risk assessment herein; it is only employed to evaluate efficiency and sufficiency of the tested *IMs* and thus acquire an early grasp on the performance of each of the candidate *IMs*. Obviously, lacking any long duration or pulse-like ground motions, all relevant conclusions should be constrained to the usual case of "ordinary" records. Figure 3 presents the response spectra of the GMset-plain as well as their longest usable periods. Records with longest usable period lower than T_c are excluded from GMset-plain to avoid biasing the ratio of spectral values in T_i versus T_c due to record processing. In addition to this record set and to maintain the hazard consistency in evaluation of the seismic risk of the case study liquid storage tanks for scalar *IMs*, Conditional Spectrum (CS, [49,50]) based record selection is adopted. For each of the candidate scalar *IMs*, a set of 30 records corresponding with its 2% in 50 years return period that best match with the CS target are selected using the algorithm of Jayaram et al. [51]. These sets are referred to as GMset-CS$_k$, where $k \in${1, 2, 3, 4, 5, 6, 7-1, 7-2, 7-3} corresponds to the indices of scalar *IMs* in Table 2. These record sets serve as the state-of-the-art input for IDA and thus the risk-based evaluation of both the individual failure modes and the (global) system-level damage states. Note that, in contrast to GMset-plain, CS selected sets were not screened for appropriate longest usable periods. The reason is that the 'Joystick' model does not include actual periods higher than T_i; T_c is only applied through post-processing and the CS selection approach guarantees that the appropriate distribution of spectral ratio between T_i and T_c is maintained.

Figure 4 summarises the CS record selection results for the majority of the considered scalar *IMs*. For each candidate *IM*, the single record spectra are presented on the first column of the panels that compose Figure 4, along with the median, 2.5th and 97.5th percentiles. The second

DOI: XX

and third columns depict the comparison between the target and sample median as well as standard deviation, respectively. Note that, to further simplify the problem, we used a single set of records for all *IM* levels to perform IDA instead of selecting multiple sets for multiple *IM* levels [10]. This may slightly bias the results presented herein because the spectral shape changes by the intensity level, nevertheless, this bias is expected to be insignificant [52]. Vector *IMs* have not received a similar comprehensive treatment of CS selection as the relevant methods are only now appearing in the literature [53,54]. Still, by nature, vector *IMs* are considered to offer higher sufficiency; thus the corresponding GMset-CS records of the primary element [i.e. PGA and $S_a(T_i)$] of IM_{v1} and IM_{v2}, respectively, are employed.

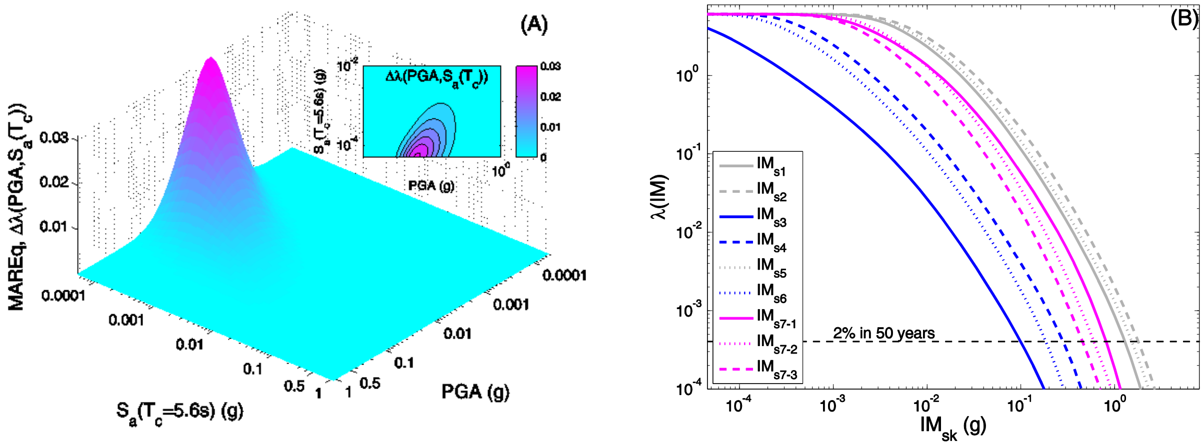

Figure 2: Probabilistic seismic hazard analysis. A, mean annual rate of equalling (MAREq) joint values of $\{PGA, S_a(T_c\text{=}5.6\text{ s})\}$, i.e. IM_{v1}; hazard surface and contour. B, mean annual frequency of exceeding IM_{sk} values, where $k \in \{1, 2, 3, 4, 5, 6, 7\text{-}1, 7\text{-}2, 7\text{-}3\}$.

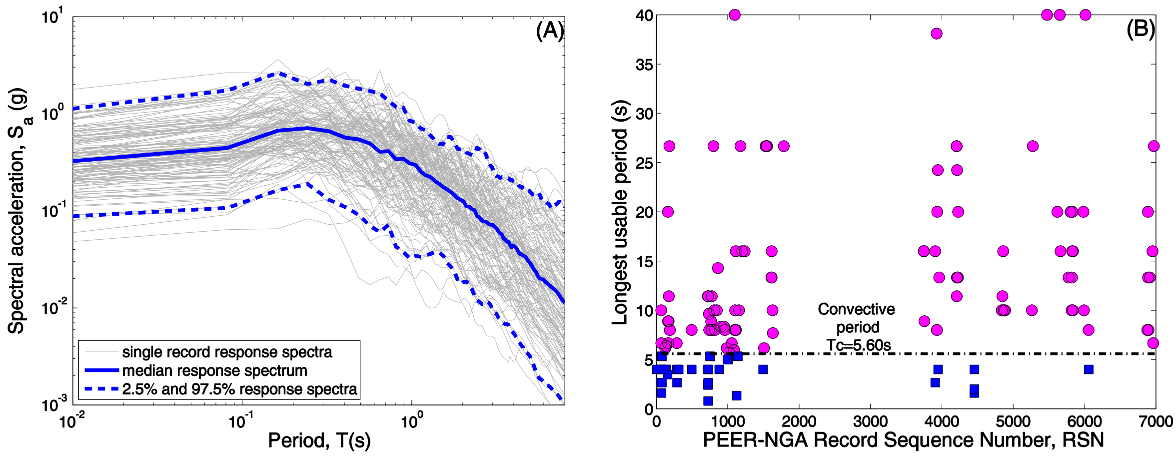

Figure 3: GMset-plain. A, spectra and B, longest usable periods versus the PEER-NGA record sequence numbers. Squares and circles indicate records with longest usable period less and greater than T_c=5.6s.

DOI: XX

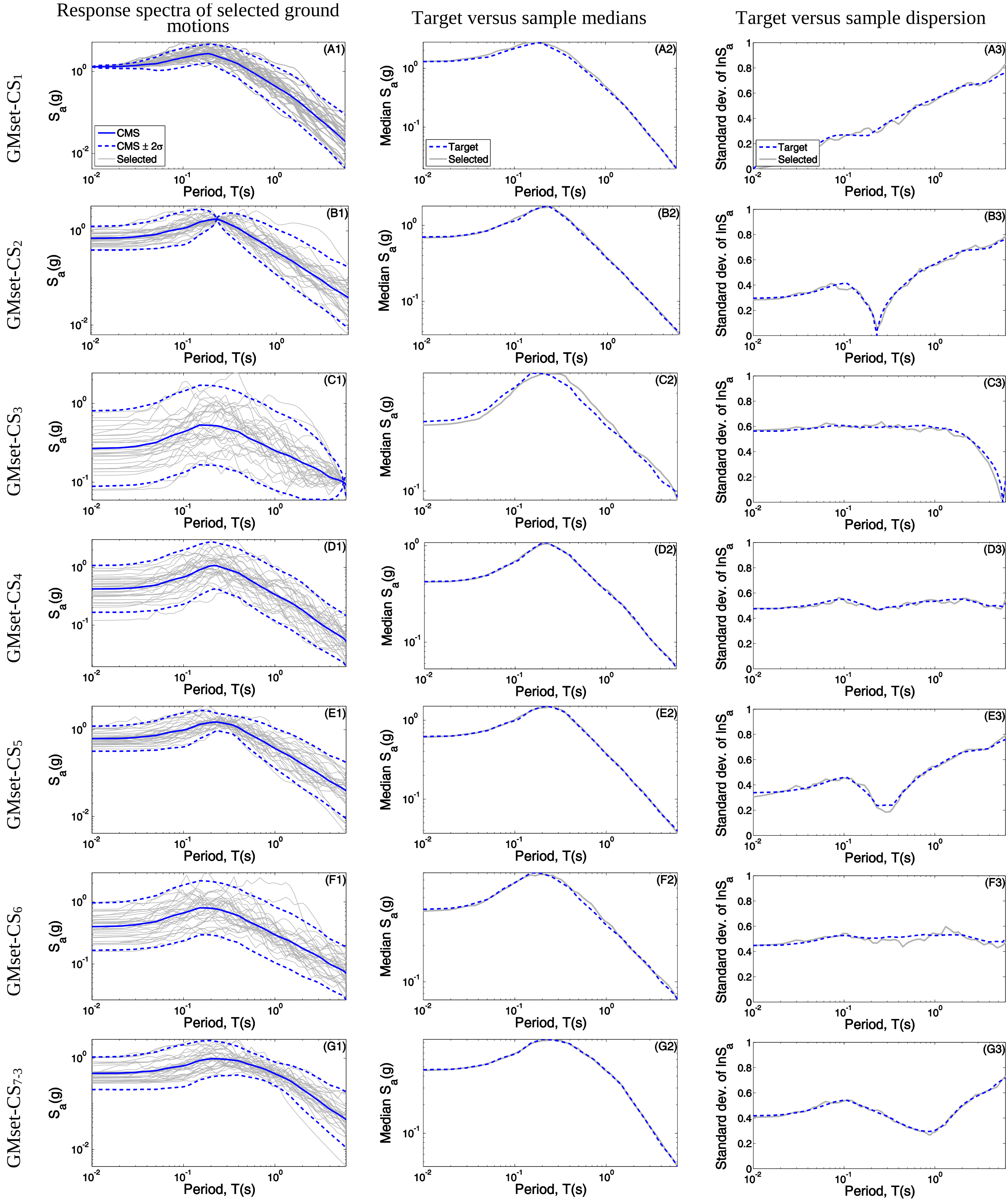

Figure 4: CS record selection for scalar *IMs* of Table 2. The left column shows the selected ground motion spectra along with the associated median (or conditional mean spectrum, CMS), 2.5th and 97.5th percentiles (CMS ± 2σ); middle and right columns show the comparison of target versus sample median and standard deviation, respectively. For brevity, only $IM_{s7\text{-}3}$ is presented from the $AvgS_a$ candidates.

DOI: XX

6. INCREMENTAL DYNAMIC ANALYSIS

Three different above-ground liquid storage tanks with aspect ratios (i.e. fluid height to radius) ranging from 0.81 to 1.76 were examined [6], in all cases arriving to similar conclusions. Herein, for the sake of brevity, only the results of a single squat tank of 1.13 aspect ratio are shown. It has a radius of R_t=13.9m, height h_t=16.5m and is 95% filled with water (i.e. fluid density ρ_f=1000kg/m^3). The thickness of the base plate is t_b=6.4mm, while that of the annular plate is t_a=8mm. A total of 9 wall courses with varying thickness is provided to form the tank shell. In particular, the thickness distribution (in mm) from the lower to the upper course of the tank is 17.7, 15.7, 13.7, 11.7, 9.7, 7.8, 6.4, 6.4 and 6.4 respectively, as shown in Figure 1A. The roof mass is m_r=35t and the material that has been used is steel S235 with a post-yield hardening ratio equal to 1%.

IDA is employed to derive the distribution of the various *EDPs* given the seismic intensity, using the GMset-plain shown in Figure 3. Each 3D analysis is conducted using both longitudinal and transverse recordings as an input. It should be noted that in the course of a preliminary investigation performed on the "Joystick" model [6], the effect of vertical ground motion component was evident on the EFB capacity only (not on any demand), and then for specific tanks and ground motion records. Therefore, it was not considered during the IDA, although the model can easily accommodate it. The process of capturing any of the aforementioned modes of failure on the "Joystick" model is presented in detail by Bakalis et al.

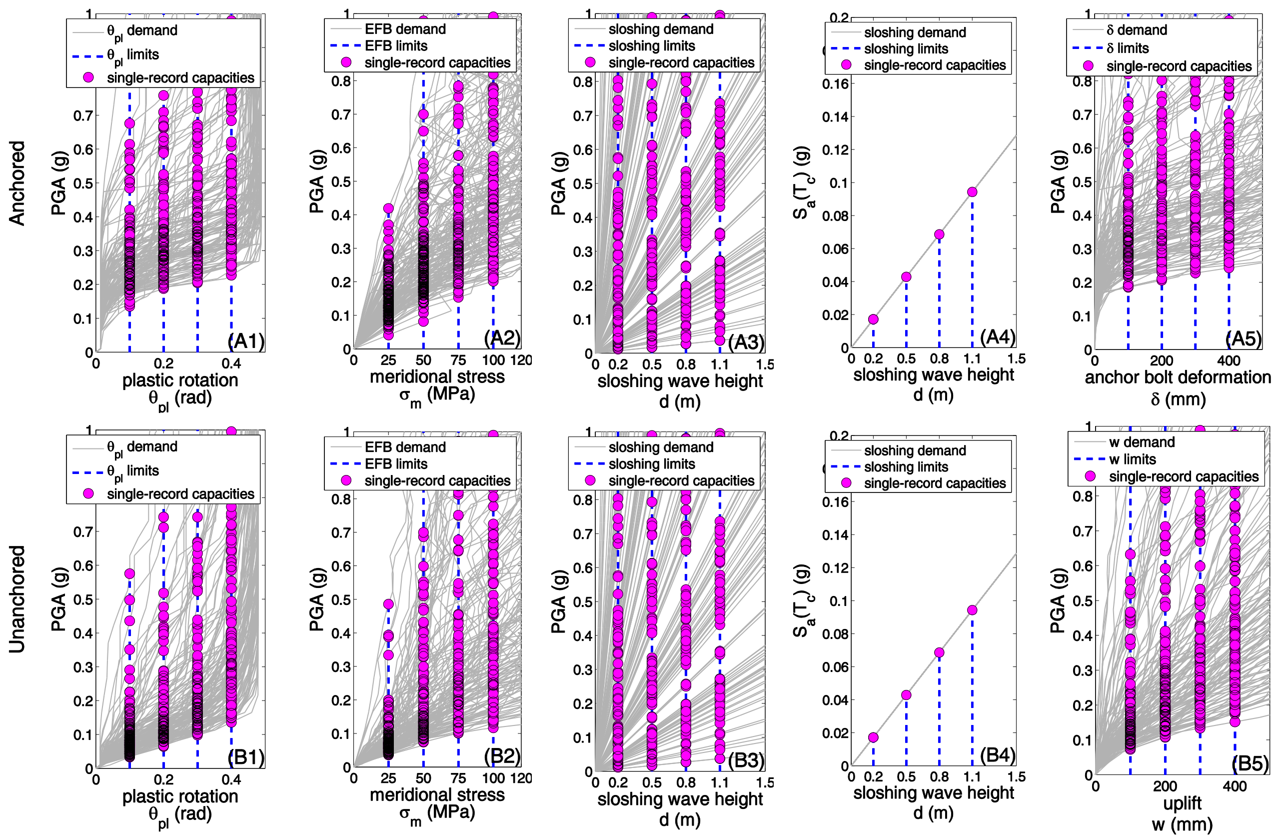

Figure 5: GMset-plain single-record IDAs and four indicative *EDP* capacities for each failure mode: A1 and B1 base plate plastic rotation, A2 and B2 meridional stress, A3, A4, B3 and B4 sloshing wave height, A5 anchor bolt deformation, B5 uplift. The results presented in row A refer to the anchored tank shown in Figure 1A, while the ones in row B to the corresponding unanchored system.

DOI: XX

in [6]. Figure 5 illustrates the single-record IDA curves for each failure mode (and thus *EDP*) of interest, along with various (potential) *EDP* capacities and the associated *IM* values that will further be exploited during the efficiency-sufficiency testing. Besides component-level *EDPs* such as plastic rotation, sloshing wave height and meridional stress, uplift is also examined for the unanchored tank in view of obtaining a wider understanding through a global response parameter. Given the dependence of the majority of failure modes on the impulsive component of the tank, the IDAs shown in the columns 1, 2 and 5 of Figure 5 indicatively adopt *PGA* as the *IM*. The sloshing wave response of Figure 5(A3, B3) also adopt *PGA* in order to display its inappropriateness (at least) in terms of efficiency, compared to $S_a(T_c)$ that is going to be a perfect predictor according to the definition of the sloshing wave height, *d* [39], as shown in Figure 5(A4, B4). It should be noted that the nonlinear-elastic response of the "Joystick" model does not allow the development of the characteristic IDA flatlines [9] that signal the global dynamic instability of the structure, where such a flatline is required, e.g. to indicate global collapse. It may be added in post-processing, still, actual collapse is mainly triggered due to the cascading/secondary effects of the earthquake (e.g. fire, tsunami) rather than the earthquake itself [3,4].

7. IM TESTING

The *IM* evaluation is performed by employing metrics of efficiency and sufficiency. In contrast to the original work of Luco and Cornell [19], whereby efficiency and sufficiency were tested singularly for the entire range of *EDP* response, the approach of Kazantzi and Vamvatsikos [29] is employed. In particular, 100 equally spaced *EDP* values are employed to determine corresponding *IM*|*EDP* capacities, termed IM_C values. These offer a high-resolution test for efficiency and sufficiency of each *EDP* and level of response. For scalar *IMs*, each set of IM_C values (i.e. for a single *EDP* threshold) appears as a vertical stripe in the typical 2D representation of IDA curves (e.g. as shown in Figure 5). For vector *IMs* of two elements, a 3D visualisation of IDA is adopted [18], whereby the first vector element [i.e. *PGA* or $S_a(T_i)$] is used to forecast the level of intensity, while the second element [i.e. $S_a(T_c)$] is normalised by the first to become a constant (Figure 6A). Then, IM_C values appear on a horizontal plane slice through the 3D IDA curves, as shown in Figure 6A, B. Therein, the additional resolution offered by a vector becomes apparent, as higher values of the *IM* ratio always indicate a more aggressive record, whereby spectral ordinates tend to increase with period. On the other hand, low values of the *IM* ratio provide little information about periods lower than T_c, where it is unknown whether they are high or low, vis-à-vis *PGA* or $S_a(T_c)$. According to the top left part of Figure 6B, extreme *IM* ratio values do indicate low IM_C capacities, and their variability is near perfectly captured (Figure 6C). Therefore, vector *IM* sufficiency and efficiency testing shall only focus on the murkier area of $S_a(T_c)/PGA<0.5$ [or $S_a(T_c)/ S_a(T_i)<0.2$] (bottom part of Figure 6B) where large variability (larger than a cut-off value of approximately 0.20) is still apparent and unexplained by any of the two vectors (IM_{v1} and IM_{v2}) employed. It should be noted that the sample of 135 IDA curves (one per record employed) shown in Figure 5 is narrowed down to 103 to comply with the aforementioned limitation in the longest usable period (Figure 3B). Furthermore, the *EDP*-response hazard curves are extracted to provide an additional source of information regarding the applicability of the candidate *IMs*, while the MAF of the compound *DS* involving both impulsive and convective-governed modes of failure are ultimately estimated in view of determining a single predictor for the risk-based evaluation of liquid storage tanks.

DOI: XX

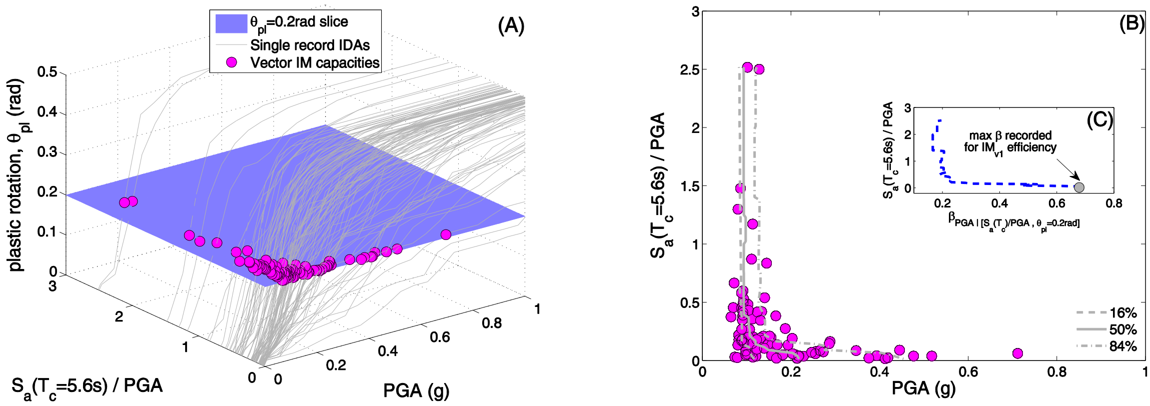

Figure 6: A, single-record IDAs based on the GMset-plain set of records for the unanchored tank of Figure 1A; plastic rotation versus the vector of {*PGA*, $S_a(T_c)/PGA$} showing the characteristic saturation of θ_{pl} at high levels of intensity [8], featuring the 0.2rad *EDP* slice. B, joint values of *PGA* and $S_a(T_c)/PGA$. C, recorded dispersion for the vector *IM* efficiency testing.

7.1. *Efficiency*

The efficiency testing for scalar *IMs* is performed by estimating the standard deviation of the 103 IM_C natural logarithm values ($\beta_{IM|EDP}$) estimated at each *EDP* level. For vector *IMs* this dispersion needs to be further conditioned on the value of $S_a(T_c)/PGA$ [or $S_a(T_c)/\ S_a(T_i)$]. Due to lack of data at every value of the vector *IM* element ratio, this conditional dispersion is evaluated by assuming lognormality and employing the 16%/50%/84% running quantiles of *PGA* [or $S_a(T_i)$] versus the corresponding ratio $S_a(T_c)/PGA$ [or $S_a(T_c)/\ S_a(T_i)$]. Then, $\beta_{IM\,|[S_a(T_c)/IM,EDP]} = 0.5\left[\ln IM^{84\%}_{S_a(T_c)/IM,EDP} - \ln IM^{16\%}_{S_a(T_c)/IM,EDP}\right]$, as indicatively shown in Figure 6B and C for θ_{pl}=0.2rad and *IM*=*PGA*. As discussed earlier, only the higher values of $\beta_{IM\,|[S_a(T_c)/IM,EDP]}$ appearing in the lower part of Figure 6C are of interest.

The results presented in Figure 7 refer to the geometry of the tank shown in Figure 1A using both anchored and unanchored support conditions. A general conclusion that can be drawn regarding the failure modes that are predominantly governed from the impulsive component of the tank (i.e. plastic rotation, EFB, uplift and anchor bolt failure), is that their capacities are less dispersed when the geometric mean of multiple spectral ordinates close to T_i is adopted as in IM_{s5} and IM_{s7} (Figure 7A1, B1, A2, B2, A4, B4). For the unanchored tank, $IM_{s7\text{-}2}$ and $IM_{s7\text{-}3}$ appear to be two potentially optimal intensity measures as they develop the smallest dispersion estimates throughout the *EDP* range considered, the former performing better for low/moderate values and the latter elsewhere. $IM_{s7\text{-}1}$ is another decent alternative, while the geometric mean of $S_a(T_i)$ and $S_a(1.5T_i)$ (=IM_{s5}) appears to be a reasonable option too, as the pertinent dispersion estimates do not fall far away from those of $IM_{s7\text{-}1}$, at least for moderate *EDP* values (e.g. θ_{pl}>0.1rad and σ_m>30MPa). Similarly, combinations of $S_a(T_i)$ and *PGA* with $S_a(T_c)$ (=IM_{s4} and IM_{s6}) may also be deemed applicable for a certain range of *EDP* values regarding plastic rotation and meridional stress [e.g. θ_{pl}>0.25rad and σ_m>50MPa, Figure 7(B1, B2)]. On the contrary, *PGA* and $S_a(T_i)$ alone (=IM_{s1} and IM_{s2}) cannot be considered acceptable predictors for the aforementioned *EDPs*, as they develop considerably larger dispersions compared to the rest of candidate *IMs*.

As far as the anchored tank is concerned, the response of impulsive controlled *EDPs* is slightly different from that of the unanchored tank. In particular, IM_{s5} stands out as a potentially optimal solution, while $S_a(T_i)$ (=IM_{s2}) appears as an acceptable alternative for certain *EDPs* (e.g.

DOI: XX

Figure 7A2 and Figure 7A1 for θ_{pl}<0.2rad). Regarding $AvgS_a$ candidates, $IM_{s7\text{-}1}$ appears to be superior compared to $IM_{s7\text{-}2}$ and $IM_{s7\text{-}3}$, for certain ranges of the *EDP* capacities considered (e.g. θ_{pl}<0.25rad and σ_m<70MPa). Once again there is no singularly optimal *IM* at all *EDP* ranges of interest. This effect is mainly evident for plastic rotation capacities that exceed 0.3rad (Figure 7A1) and anchor bolt deformations larger than the prescribed fracture capacity of 100mm (Figure 7A4), although Figure 7A2 implies that a similar effect would be observed for EFB should σ_m capacities over 100MPa were examined. Such an effect suggests that failure of anchors on a single spoke of the 'Joystick' model changes the response considerably, where the system begins to exhibit partial rocking [8], an effect that is difficult to capture using a single *IM* throughout the response range.

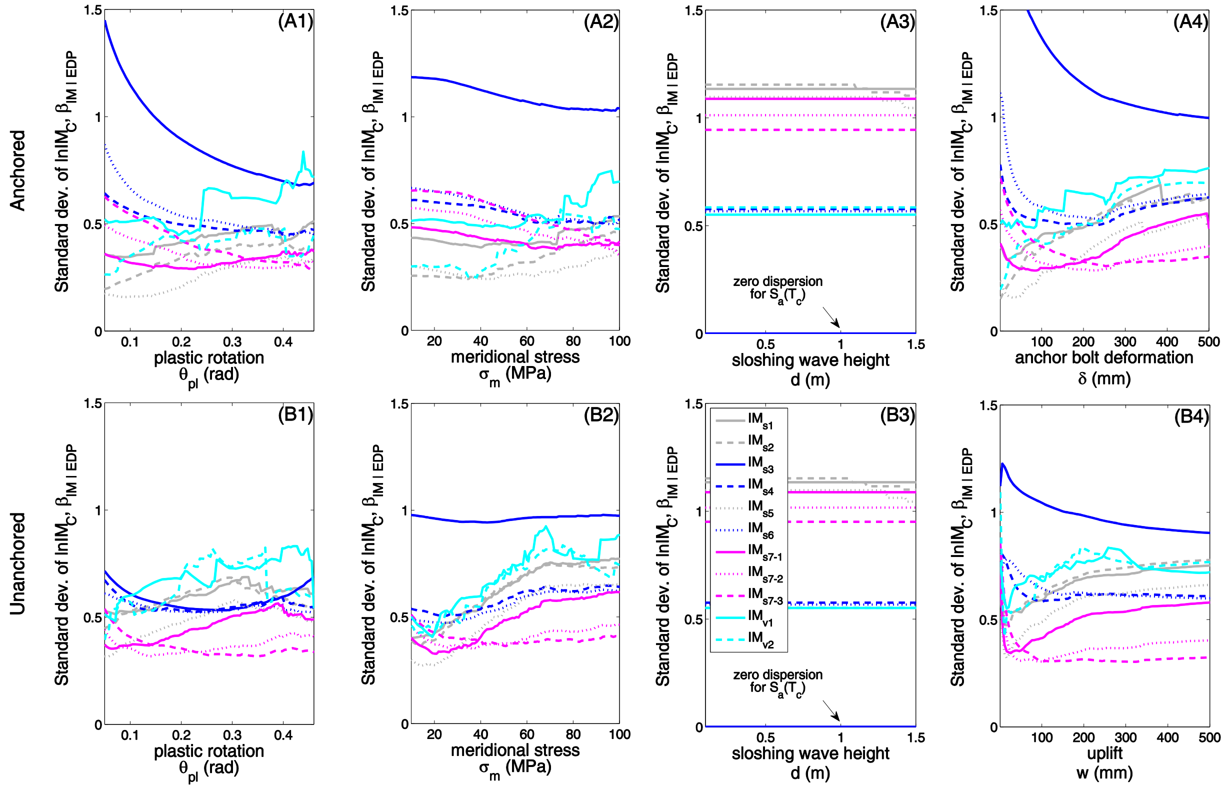

Figure 7: *IM* efficiency testing: A1 and B1 base plate plastic rotation, A2 and B2 meridional stress, A3, A4, B3 and B4 sloshing wave height, A5 anchor bolt deformation, B5 uplift. The results presented in row A refer to the anchored tank shown in Figure 1A, while the ones in row B to the corresponding unanchored system. IDA results using GMset-plain.

Regardless of anchorage conditions, vector *IMs* appear to be following the trend of their respective primary element [i.e. *PGA* or $S_a(T_i)$] for impulsive-controlled modes of failure, occasionally providing larger dispersion estimates due to the conservative criterion presented in Figure 6C. On the other hand, $S_a(T_c)$ (=IM_{s3}) appears to be the only *IM* that can efficiently predict the response related to the convective component of the tank (Figure 7A3, B3), thus confirming the initial speculations outlined in the *IM* selection section. It is also evident that nearly all other candidate *IMs* develop considerably larger dispersion estimates of sloshing, an issue which is partially solved when certain spectral ordinates are combined with $S_a(T_c)$ (e.g. IM_{s4}, IM_{s6}, $IM_{s7\text{-}3}$, IM_{v1} and IM_{v2}), but still clearly deviates from the optimal solution of $S_a(T_c)$ (=IM_{s3}).

DOI: XX

7.2. Sufficiency

Sufficiency aims to ensure that an *IM* is independent of seismological parameters such as epsilon and moment magnitude. Quantifying sufficiency is often performed via a linear regression of lnIM_C values against the aforementioned seismological characteristics as

$$\ln IM_C = a_M + b_M M_w + e_M \tag{4}$$

$$\ln IM_C = a_\varepsilon + b_\varepsilon \varepsilon + e_\varepsilon \tag{5}$$

where b_ε, b_M are the slopes, a_ε, a_M the intercepts and e_ε, e_M the normally distributed errors of these two straight lines in log space. Sufficiency essentially determines the statistical significance of each *IM* and is quantified by extracting there levant p-value from the regression output. Based on an earlier discussion for vector *IMs*, only IM_C values below the cut-off value of $S_a(T_c)/PGA$=0.5 or $S_a(T_c)/S_a(T_i)$=0.2 are employed in Equations (4) and (5).As an example, Figure 8 presents the linear regression of *PGA* values conditioned on the θ_{pl} capacity of 0.2rad versus ε and M_w, which constitutes the backbone of the process [19] that is used to generate the results that are further presented in Figures 9 and 10. It should be noted that p-values higher than 0.05 are generally acceptable indicators of low statistical significance and thus high *IM* sufficiency [19].

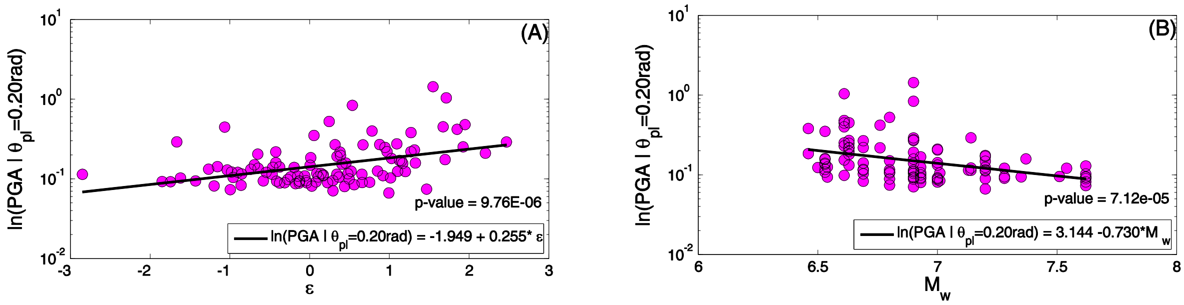

Figure 8: Linear regression of ln($PGA|\theta_{pl}$=0.20rad) values versus A, ε and B, M_w for the unanchored tank of Figure 1A

According to Figures 9 and 10, all *EDPs* besides sloshing wave height seem to be suffering from low p-values, when either of the *PGA* (=IM_{s1}), $S_a(T_i)$ (=IM_{s2}), $S_a(T_c)$ (=IM_{s3}), the geometric mean of $S_a(T_i)$ with $S_a(T_c)$ (=IM_{s4}), and that of $S_a(T_i)$ with $S_a(1.5T_i)$ (=IM_{s5}) is adopted as the *IM*, even though the latter presents acceptable p-values for the anchored tank prior to the fracture of the respective anchors, an effect that is also obvious for the $AvgS_a$ candidates $IM_{s7\text{-}2}$ and $IM_{s7\text{-}3}$. In general, $IM_{s7\text{-}1}$ appears as the most sufficient solution for the anchored system, bearing in mind that its sufficiency with respect to M_w is ensured only up to the point where anchors fracture. For the unanchored system on the other hand, $AvgS_a$ (=IM_{s7}), S_a combinations containing $S_a(T_c)$ (=IM_{s4} or IM_{s6}) and the vector *IMs* provide acceptable p-values for certain ranges of *EDP* capacities only, even though the former appears to be highly dependent on the range of periods considered for each $AvgS_a$, particularly when testing for M_w.

In any case, the p-values of Figures 9 and 10 do not point towards a single *IM* that is sufficient for the entire range of the response. At the same time, one should also bear in mind the several instances found in the literature where the use/interpretation of p-values is strongly criticised (e.g. [29,55]). This is a common issue within the scientific community, which is often attributed to the confusion of two completely different terms such as *significance* and *relevance*. Undeniably, a small p-value might be an indicator of *IM* dependence (in our case) with M_w or ε, yet the extent of this effect remains unknown. Therefore, the question one should be asking

DOI: XX

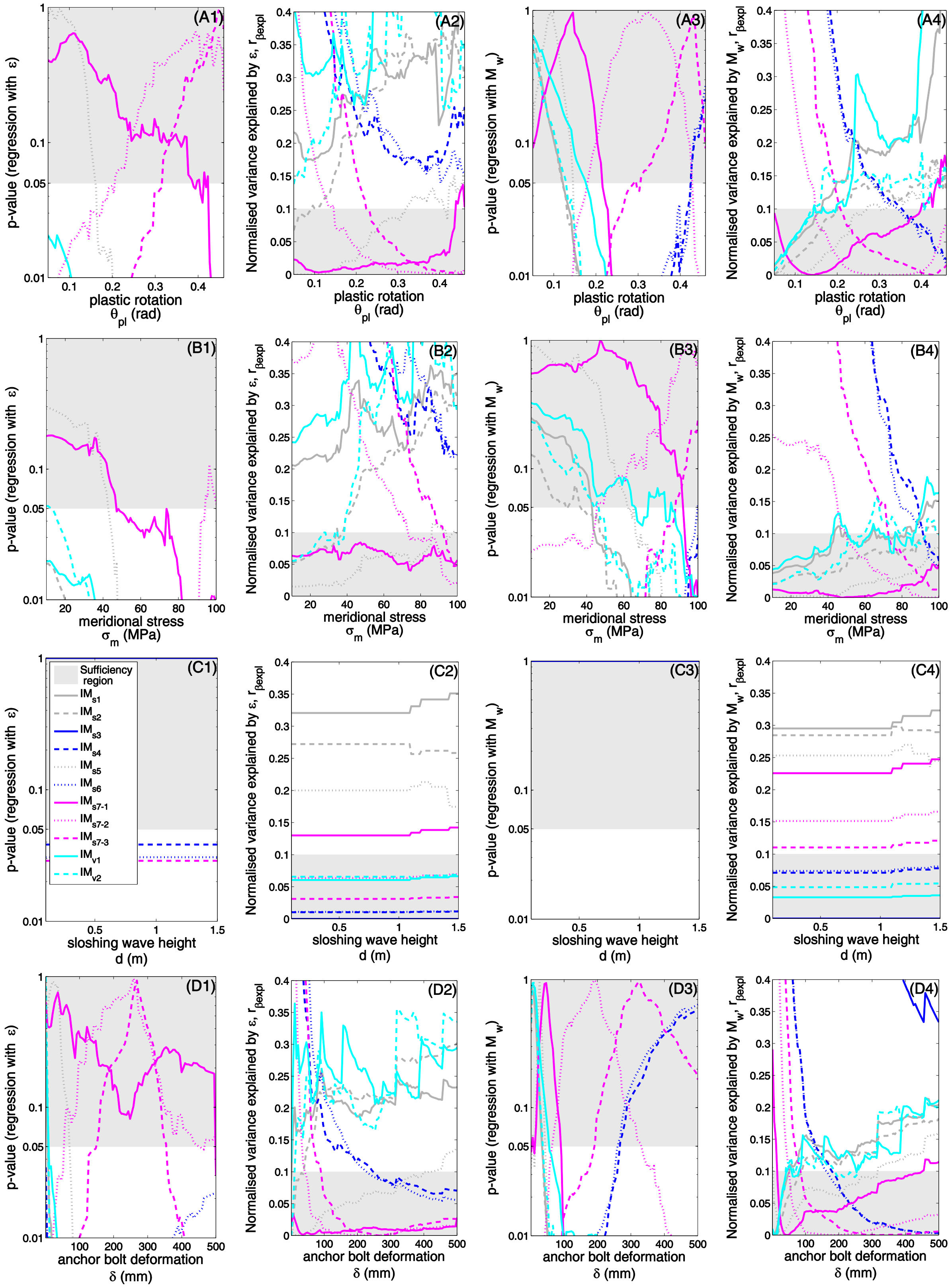

Figure 9: *IM* sufficiency for the *EDPs* of the anchored tank of Figure 1A using the GMset-plain; the columns from left to right present the p-values when the regression is performed against ε, the variance explained by ε normalised to the total $S_a(T_i)$ variance, the p-values when the regression is performed against M_w and the variance explained by M_w normalised to the total $S_a(T_i)$ variance, respectively.

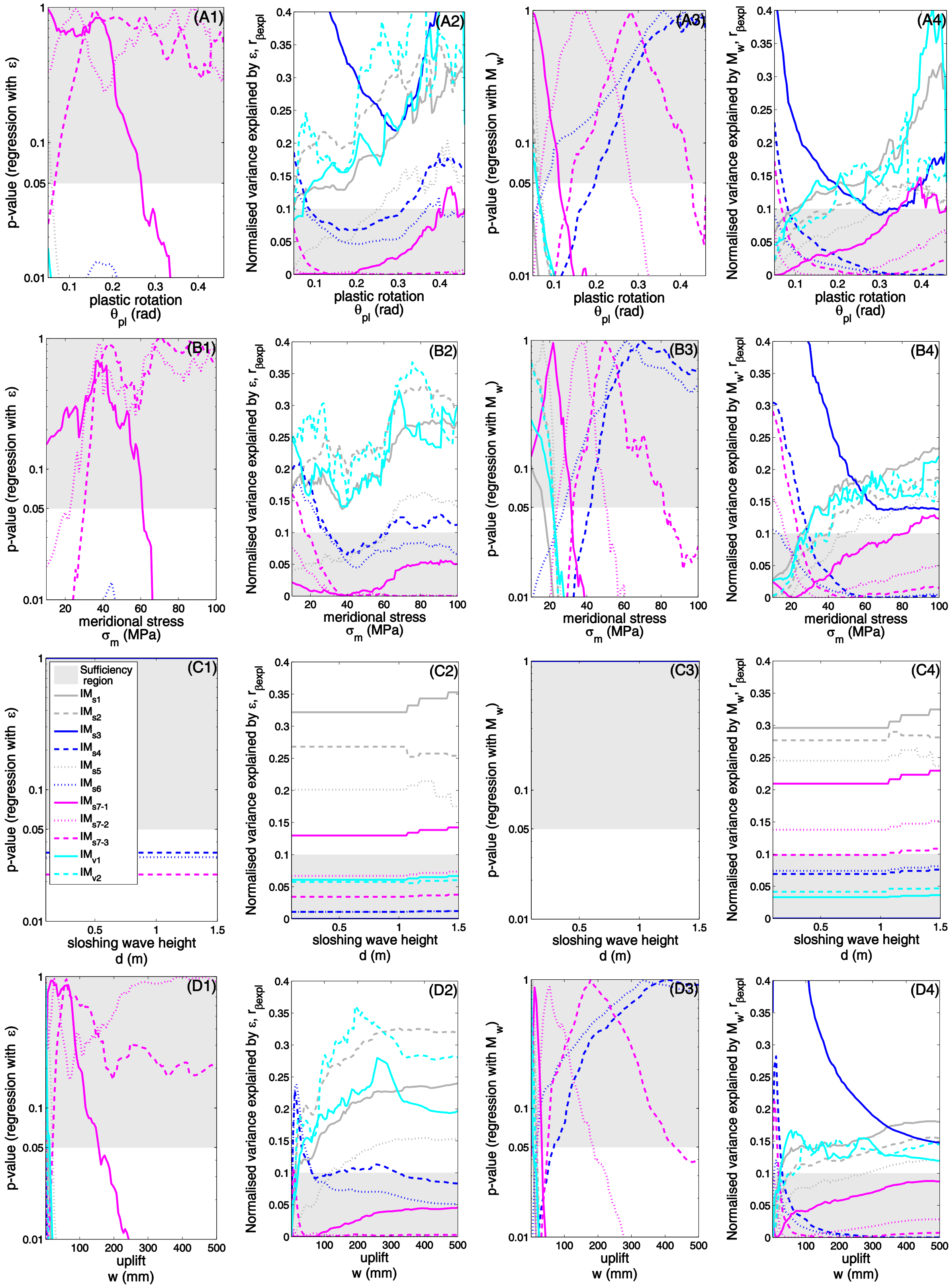

Figure 10: *IM* sufficiency for the *EDPs* of the unanchored tank of Figure 1A using the GMset-plain; the columns from left to right present the p-values when the regression is performed against ε, the variance explained by ε normalised to the total $S_a(T_i)$ variance, the p-values when the regression is performed against M_w and the variance explained by M_w normalised to the total $S_a(T_i)$ variance, respectively.

ought to be in the context of magnitude of the effect rather than the effect itself. For example, one could easily improve all p-values by using a smaller set of records, thus removing statistical significance via inadequate sampling rather than an improved *IM*. Along these lines, the authors decided to provide an alternative metric of *IM* sufficiency, i.e. the variance explained (β^2_{expl}) by ε (or M_w) normalised to the total variance of $S_a(T_i)$, $r_{\beta expl}$, or normalised variance explained by ε (or M_w) in short

$$r_{\beta expl} = \frac{\beta^2_{expl}}{\beta^2_{S_a(T_i)|EDP}} = \frac{R^2 \beta^2_{IM|EDP}}{\beta^2_{S_a(T_i)|EDP}}. \tag{6}$$

The variance explained, β^2_{expl}, is estimated via the coefficient of determination (R^2) equation as

$$R^2 = 1 - \frac{SSE}{TSS} = \frac{TSS - SSE}{TSS} = \frac{\beta^2_{IM|EDP} - \beta^2_{error}}{\beta^2_{IM|EDP}} = \frac{\beta^2_{expl}}{\beta^2_{IM|EDP}} \Leftrightarrow \beta^2_{expl} = R^2 \beta^2_{IM|EDP},$$

where $TSS = \beta^2_{IM|EDP}$ is the total sum of squares (or the variance of $IM|EDP$), $SSE = \beta^2_{error}$ is the error sum of squares, and their difference is the variance explained. $r_{\beta expl}$, similar in principle to other metrics proposed in the literature (e.g. the relative sufficiency measure of Jalayer et al. [56,57]), describes the proportion by which the variance of the prediction errors shrinks, and is estimated herein using the product of the coefficient of determination (R^2) and the total IM_C variance, over the total variance of $S_a(T_i)$ capacities. In essence, low variance-explained values (e.g. < 0.10) imply *IM* sufficiency, meaning that M_w or ε do not offer any appreciable change to the determination of IM_C, thus their omission does not bias the relevant fragility (i.e. cumulative distribution function of IM_C). Therefore, according to Figures 9 and 10, the $AvgS_a$ $IM_{s7\text{-}1}$ is clearly promoted as the best option available for impulsive-driven modes of failure of anchored tanks, while all $AvgS_a$ are viable candidates for unanchored tanks. It should be noted that the aforementioned *IMs* as well as the vectors considered seem to be working for sloshing wave height too, only in absence of $S_a(T_c)$ (=IM_{s3}), though, which is by default the optimal solution in this particular case.

7.3. *EDP-hazard*

A further comparison among the candidate *IMs* is performed by extracting the response hazard curves for the *EDPs* of interest through Equation (1). The results presented in Figure 11 refer to the tank shown in Figure 1A, using both anchored and unanchored support conditions, for each of the *IMs* outlined in Table 2. Discrepancies among the various response hazard curves are evident, especially for the impulsive-controlled modes of failure. On the other hand, sloshing wave height MAFs appear to be less dispersed when different scalar *IMs* are employed, thus implying that the seismic risk evaluation of this particular *EDP* is essentially unaffected by the *IM*, an argument that obviously needs a considerable amount of data to be supported for tank configurations other than the one examined herein (e.g. non-squat). Shape-wise, for anchored support conditions, the plastic rotation hazards (Figure 11A1) seem to display characteristic changes in steepness in the range of 0.02-0.05rad, which can be attributed to the sudden increase in dispersion, stemming from the uplift that the system begins to exhibit.

Overall, comparing the *EDP*-hazards for various candidate intensity measures cannot offer any significant insight on its own, as it essentially lacks a baseline solution, which means that any scatter observed among them may only be attributed to epistemic uncertainty inherent in the state-of-the-art approach of employing CS selection to remove any *IM* insufficiency. *EDP*-hazard curves are certainly useful to distinguish the outliers among the candidate *IMs*, combined to other relevant information such as efficiency and sufficiency (Figures 7, 9 and 10). Along

DOI: XX

these lines, PGA (=IM_{s1}) and $S_a(T_c)$ (=IM_{s3}) may be deemed unfit predictors for the evaluation of impulsive-controlled modes of failure, while at the same time it should be noted that the $AvgS_a$ candidates (=IM_{s7}) appear to serve as the central value among the rest of candidate *IMs*, regardless of the *EDP*.

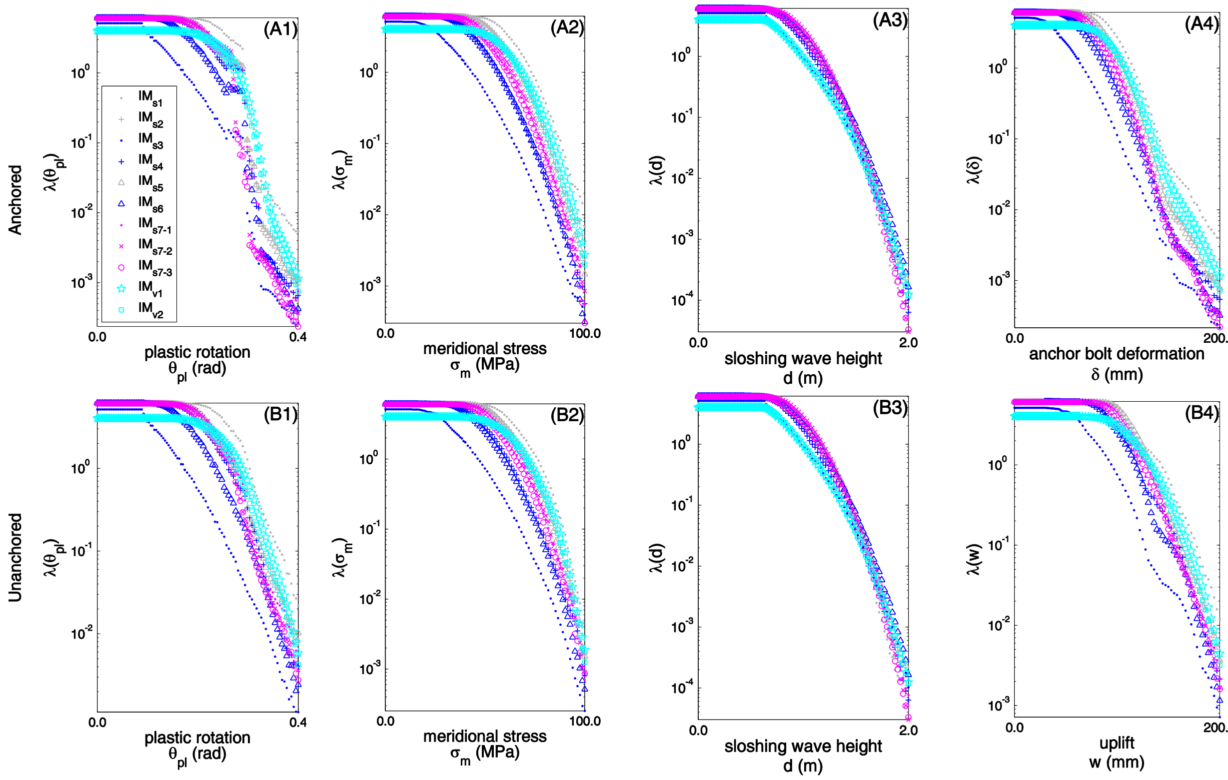

Figure 11: *EDP* hazard curves featuring the *IMs* of Table 2. A1 and B1 base plate plastic rotation, A2 and B2 meridional stress, A3 and B3 sloshing wave height, A4 anchor bolt deformation, B4 uplift. The results presented in row A refer to the anchored tank of Figure 1A, while the ones in row B to the corresponding unanchored system. IDA results for GMset-CS.

7.4. Compound damage states

The information outlined so far is useful for the assessment of modes of failure determined by a single *EDP*. Still, it provides little insight on the issue of compound system-level damage states, controlled by two or more *EDPs*, as for example *DS*2. The latter is defined as the union of two and three events for unanchored and anchored tanks, respectively, involving both impulsive and convective modes of failure (Table 1). The latter, for the case of vector *IM* candidates, implies the necessity to generate the fragility surfaces appearing in Figure 12 for anchored and unanchored tanks, estimated by adopting a lognormal assumption in conjunction with the running quantiles of Figure 6B at each *EDP* level.

Due to specific definition of *DS*2 and the near-zero correlation among spectral ordinates at the widely spaced periods of T_i and T_c [58,59], one may achieve a decomposition of the fragility and the MAF estimate for a 2-component vector IM_v={IM_A, IM_B}, thus proposing a computationally cheap in terms of site hazard analysis alternative. For a union of two events *A*, *B*, each depending solely on IM_A, IM_B, respectively, this becomes

$$\begin{aligned}\lambda_{DS,IM_v} &= \iint \mathrm{P}\left(DS \mid IM_A, IM_B\right)\mathrm{d}\lambda\left(IM_A, IM_B\right)\\ &= \sum_p \sum_q \mathrm{P}\left(DS \mid IM_A^p, IM_B^q\right)\Delta\lambda\left(IM_A^p, IM_B^q\right)\\ &\approx \sum_p \sum_q \left[\mathrm{P}\left(A \mid IM_A^p, IM_B^q\right) + \mathrm{P}\left(B \mid IM_A^p, IM_B^q\right) - \mathrm{P}\left(A \mid IM_A^p, IM_B^q\right)\mathrm{P}\left(B \mid IM_A^p, IM_B^q\right)\right]\Delta\lambda\left(PGA_p, S_a\left(T_c\right)_q\right)\end{aligned}$$

where P[$DS|IM_A$, IM_B] is the corresponding fragility surface. Due to failure modes A, B being dependent only on a single IM, the double sum (or integral) involving a second irrelevant quantity simplifies to the classic scalar IM sum (or integral) of Equation (1). Thus:

$$\lambda_{DS,IM_v} \approx \lambda_{A,IM_A} + \lambda_{B,IM_B} - \lambda_{A,IM_A}\lambda_{B,IM_B} \tag{7}$$

Similarly, for a DS being a 3-event union of A, B, C, dependent on IM_A, IM_B, IM_A, respectively:

$$\lambda_{DS,IM_v} \approx \lambda_{A,IM_A} + \lambda_{B,IM_B} + \lambda_{C,IM_A} - \lambda_{A,IM_A}\lambda_{B,IM_B} - \lambda_{A,IM_A}\lambda_{C,IM_A} - \lambda_{B,IM_B}\lambda_{C,IM_A} + \lambda_{A,IM_A}\lambda_{B,IM_B}\lambda_{C,IM_A} \tag{8}$$

Equations (7) and (8) are essentially the intersection probability of two and three events in MAF space, respectively.

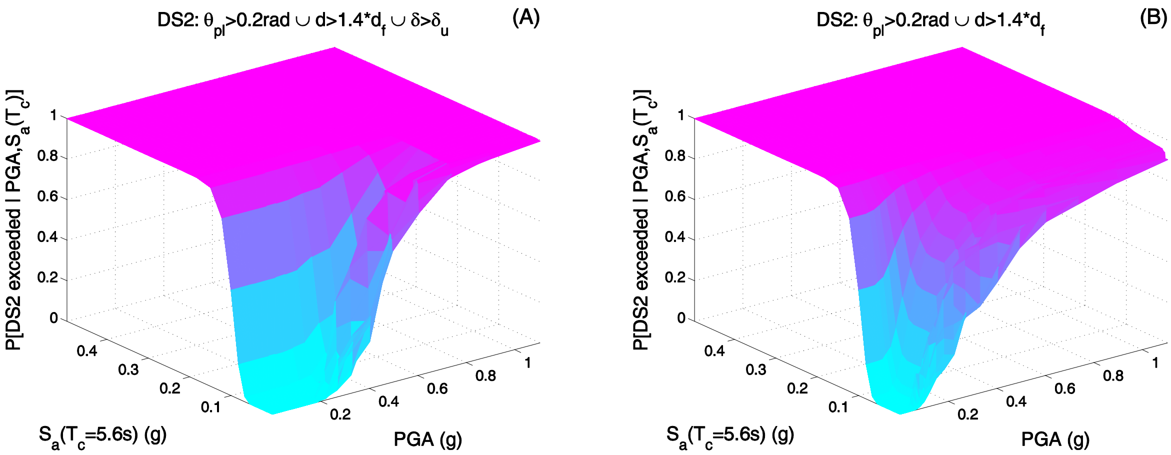

Figure 12: Probability of exceeding $DS2$ versus IM_{v1}. A, anchored and B, unanchored support conditions.

A comparison among the $DS2$ MAFs ($\lambda_{DS2,IM}$) is presented in Figure 13 with respect to the candidate IMs examined so far. Given that $DS2$ consists of a union of events that involve both impulsive and convective-controlled modes of failure (Table 1), the vector-valued IM_{v2} is indicatively adopted as a baseline solution thanks to its (slightly) better performance over IM_{v1}. Thus, the $DS2$ MAFs are normalised with respect to the corresponding MAF value $\lambda_{DS2,IMv2}$. As expected (Figures 7 and 11), Figure 13 reveals poor behaviour of the PGA (=IM_{s1}) for both anchored and unanchored support conditions, with respect to IM_{v2}. For the unanchored system, IM_{v1} and $IM_{v1,\mathrm{Eq}(7)}$ reveal a response similar to the PGA (=IM_{s1}), thus highlighting its dominant effect on the vector-valued IM. On the other hand, $S_a(T_i)$ (=IM_{s2}), IM_{s5}, the $AvgS_a$ candidates (=IM_{s7}) and the solution proposed through Equation (8) appear to be very close to the baseline solution of IM_{v2}. For the anchored system, however, there is no obvious candidate to be named as optimal. Actually, due to the change in system behaviour introduced by fracturing anchors, one cannot claim that IM_{v2}, which is neither efficient (Figure 7) nor sufficient (Figure 9), is an optimal choice. It is still employed as a baseline solution in this case to preserve consistency in

DOI: XX

the comparison of the pertinent *IMs* and structural systems (i.e. anchored versus unanchored), bearing in mind that a vector of $AvgS_a$ and $S_a(T_c)$ might be a good way to get relatively efficient and sufficient results, at least if combined with a simple approximation that eliminates the need for a fragility surface and VPSHA. Considering those limitations, the sole outcome that can be drawn from Figure 13A is that the $AvgS_a$ candidates (=IM_{s7}) provide similar MAF estimates for *DS*2, and may thus be deemed appropriate. Also, the simplified estimate of Equations (7) and (8) is matching the results at least for IM_{v2}, offering a simpler way of employing vector *IMs* for tank assessment.

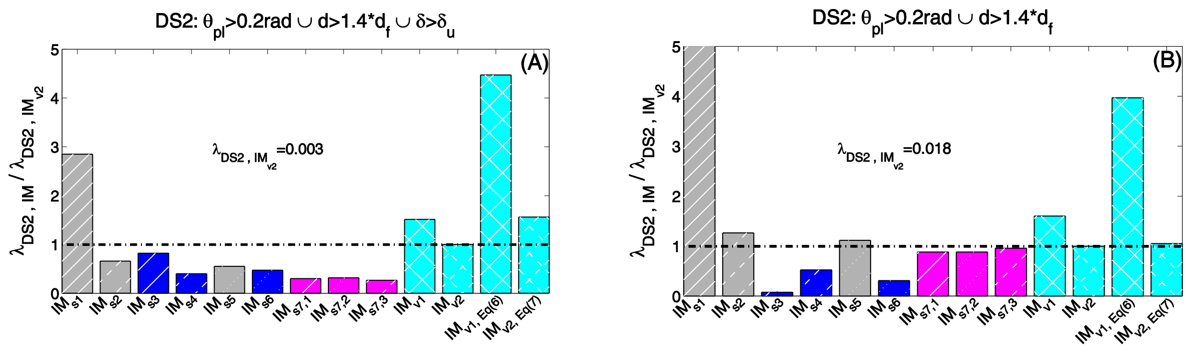

Figure 13: *DS*2 mean annual frequencies normalised to that of IM_{v2} for all candidate *IMs*. A, anchored and B, unanchored support conditions.

8. CONCLUSIONS

The applicability of several seismic intensity measures has been demonstrated for the seismic risk assessment of a squat liquid storage tank that is examined both under anchored and unanchored support conditions. Given that the motivation of this study is to propose an *IM* that is predominately able to reliably estimate the seismic risk for damage that is mutually controlled by the impulsive and convective fluid components of the tank, a dilemma/challenge arises regarding the nature of the *IM* that should eventually be nominated. On one hand, it is fairly obvious that the aforementioned problem can be adequately described using a vector of *IMs*, which admittedly is not very handy within the context of loss estimation due to the VPSHA and the fragility surface it demands; on the other hand, scalar *IMs* may need to be overly complex to achieve an acceptable solution for such diverse structural response, thus requiring a 'trial and error' process similar to the quest for suitable predictors in regression.

Altogether, the substantial difference in response for tanks with anchored and unanchored support conditions does not encourage the nomination of a single *IM* for their simultaneous seismic risk assessment, e.g. in a tank farm. For unanchored tanks, a potentially optimal solution is the average spectral acceleration $AvgS_a$ for a period range of [0.1s, 4.5T_i], while other similar period ranges or geometric mean combinations of T_i and 'elongated' T_i ordinates also perform reliably. For anchored tanks, the fracture of anchors clearly separates the response into two different regions, whereby pre-fracture assessment is better performed with the geometric mean of $S_a(T_i)$ and $S_a(1.5T_i)$ (an elastoplastic system), while post-fracture, one of the $AvgS_a$ candidates works well (a nonlinear elastic system). In addition, vector *IMs* can be employed with ease without vector PSHA and surface fragility burdens, by adopting a simple approximation for potentially superior efficiency and sufficiency.

Besides the outcome of this study itself, it is worth discussing the procedure that has been followed in order to reach the aforementioned conclusion. Each of the metrics that have been

DOI: XX

adopted for the *IM* evaluation provides useful information. For instance, dispersion in response offers an indication of *IM* efficiency, p-values are traditionally used to test sufficiency, while variance explained appears as a more reliable test for the latter, as it is not adversely influenced by the number of data points or the efficiency of the *IM*. The problem is that none of these metrics can stand on its own, which is quite intriguing, as individual parameters such as efficiency may fulfil the requirements to let a candidate *IM* be promoted as a potentially optimal solution, yet the cross examination with sufficiency for instance may indicate otherwise (although this is known to be a very rare scenario). Still, even in the case where all these properties are well within the allowable limits, the lack of a crystal-clear baseline solution may create additional obstacles in determining the optimal solution, as for instance in the case of *DS*2 for the anchored tank examined herein. In any case, the procedure that has been presented is straightforward, and the results could further be refined upon the availability of more reliable (or better studied) fracture capacities of the anchors.

REFERENCES

1. Cornell CA, Krawinkler H. Progress and Challenges in Seismic Performance Assessment. *PEER Center News* 2000; **3**(2): 1–4.
2. Thoms EE, Haeussler PJ, Anderson RD, McGimsey RG. *1964 Great Alaska Earthquake—A Photographic Tour of Anchorage, Alaska*. U.S. Geological Survey Open-File Report 2014-1086, 48 P.: 2014. DOI: 10.3133/ofr20141086.
3. Girgin S. The natech events during the 17 August 1999 Kocaeli earthquake: aftermath and lessons learned. *Natural Hazards and Earth System Science* 2011; **11**(4): 1129–1140. DOI: 10.5194/nhess-11-1129-2011.
4. Hatayama K. Damage to Oil Storage Tanks from the 2011 Mw 9.0 Tohoku-Oki Tsunami. *Earthquake Spectra* 2015; **31**(2): 1103–1124. DOI: 10.1193/050713EQS120M.
5. RASOR. Risk Assessment for the Seismic protection Of industRial facilities, THALES 2015. http://excellence.minedu.gov.gr/thales/en/thalesprojects/379422.
6. Bakalis K, Vamvatsikos D, Fragiadakis M. Seismic risk assessment of liquid storage tanks via a nonlinear surrogate model. *Earthquake Engineering & Structural Dynamics* 2017; **46**(15): 2851–2868. DOI: 10.1002/eqe.2939.
7. Vathi M, Karamanos SA, Kapogiannis IA, Spiliopoulos K V. Performance Criteria for Liquid Storage Tanks and Piping Systems Subjected to Seismic Loading. *Journal of Pressure Vessel Technology* 2017; **139**(5): 51801. DOI: 10.1115/1.4036916.
8. Bakalis K, Fragiadakis M, Vamvatsikos D. Surrogate Modeling for the Seismic Performance Assessment of Liquid Storage Tanks. *Journal of Structural Engineering* 2017; **143**(4): 4016199. DOI: 10.1061/(ASCE)ST.1943-541X.0001667.
9. Vamvatsikos D, Cornell CA. Incremental dynamic analysis. *Earthquake Engineering & Structural Dynamics* 2002; **31**(3): 491–514. DOI: 10.1002/eqe.141.
10. Jalayer F. Direct Probabilistic Seismic Anaysis: Implementing Non-linear Dynamic Assessments. Ph.D. dissertation, Dept. of Civil and Environmental Engineering, Stanford Univ., Stanford, CA, 2003.
11. Eads L, Miranda E, Krawinkler H, Lignos DG. An efficient method for estimating the collapse risk of structures in seismic regions. *Earthquake Engineering & Structural Dynamics* 2013; **42**(1): 25–41. DOI: 10.1002/eqe.2191.
12. Cornell CA. Engineering Seismic Risk Analysis. *Bulletin of the Seismological Society of America* 1968; **58**(5): 1583–1606.
13. Malhotra PK. Practical Nonlinear Seismic Analysis of Tanks. *Earthquake Spectra* 2000; **16**(2): 473–492. DOI: 10.1193/1.1586122.
14. Spritzer JM, Guzey S. Review of API 650 Annex E: Design of large steel welded aboveground storage tanks excited by seismic loads. *Thin-Walled Structures* 2017; **112**(September): 41–65. DOI: 10.1016/j.tws.2016.11.013.
15. Ozdemir Z, Souli M, M. Fahjan Y. Numerical Evaluation of Nonlinear Response of Broad Cylindrical

Steel Tanks under Multidimensional Earthquake Motion. *Earthquake Spectra* 2012; **28**(1): 217–238. DOI: 10.1193/1.3672996.

16. Phan HN, Paolacci F. Efficient Intensity Measures for Probabilistic Seismic Response Analysis of Anchored Above-Ground Liquid Steel Storage Tanks. *Volume 5: High-Pressure Technology; Rudy Scavuzzo Student Paper Symposium and 24th Annual Student Paper Competition; ASME Nondestructive Evaluation, Diagnosis and Prognosis Division (NDPD); Electric Power Research Institute (EPRI) Creep Fatigue Workshop*, vol. 5, ASME; 2016. DOI: 10.1115/PVP2016-63103.
17. Phan HN, Paolacci F, Bursi OS, Tondini N. Seismic fragility analysis of elevated steel storage tanks supported by reinforced concrete columns. *Journal of Loss Prevention in the Process Industries* 2017; **47**(2017): 57–65. DOI: 10.1016/j.jlp.2017.02.017.
18. Vamvatsikos D, Cornell CA. Developing efficient scalar and vector intensity measures for IDA capacity estimation by incorporating elastic spectral shape information. *Earthquake Engineering and Structural Dynamics* 2005; **34**(13): 1573–1600. DOI: 10.1002/eqe.496.
19. Luco N, Cornell CA. Structure-Specific Scalar Intensity Measures for Near-Source and Ordinary Earthquake Ground Motions. *Earthquake Spectra* 2007; **23**(2): 357–392. DOI: 10.1193/1.2723158.
20. Giovenale P, Cornell CA, Esteva L. Comparing the adequacy of alternative ground motion intensity measures for the estimation of structural responses. *Earthquake Engineering & Structural Dynamics* 2004; **33**(8): 951–979. DOI: 10.1002/eqe.386.
21. Padgett JE, Nielson BG, DesRoches R. Selection of optimal intensity measures in probabilistic seismic demand models of highway bridge portfolios. *Earthquake Engineering & Structural Dynamics* 2008; **37**(5): 711–725. DOI: 10.1002/eqe.782.
22. Kohrangi M, Bazzurro P, Vamvatsikos D. Vector and Scalar IMs in Structural Response Estimation, Part II: Building Demand Assessment. *Earthquake Spectra* 2016; **32**(3): 1525–1543. DOI: 10.1193/053115EQS081M.
23. Tothong P, Luco N. Probabilistic seismic demand analysis using advanced ground motion intensity measures. *Earthquake Engineering & Structural Dynamics* 2007; **36**(13): 1837–1860. DOI: 10.1002/eqe.696.
24. Tothong P, Cornell CA. Structural performance assessment under near-source pulse-like ground motions using advanced ground motion intensity measures. *Earthquake Engineering & Structural Dynamics* 2008; **37**(7): 1013–1037. DOI: 10.1002/eqe.792.
25. Baker JW, Cornell CA. Which spectral acceleration are you using? *Earthquake Spectra* 2006; **22**(2): 293–312. DOI: 10.1193/1.2191540.
26. Cordova P, Deierlein G, Mehanny SF, Cornell CA. Development of a two-parameter seismic intensity measure and probabilistic design procedure. *The Second U.S.- Japan Workshop on Performance-Based Earthquake Engineering Methodology for Reinforced Concrete Building Structures*, Sapporo, Hokkaido: 2001.
27. Eads L, Miranda E, Lignos DG. Average spectral acceleration as an intensity measure for collapse risk assessment. *Earthquake Engineering & Structural Dynamics* 2015; **44**(12): 2057–2073. DOI: 10.1002/eqe.2575.
28. Kohrangi M, Vamvatsikos D, Bazzurro P. Site dependence and record selection schemes for building fragility and regional loss assessment. *Earthquake Engineering & Structural Dynamics* 2017; **46**(10): 1625–1643. DOI: 10.1002/eqe.2873.
29. Kazantzi AK, Vamvatsikos D. Intensity measure selection for vulnerability studies of building classes. *Earthquake Engineering & Structural Dynamics* 2015; **44**(15): 2677–2694. DOI: 10.1002/eqe.2603.
30. Bojórquez E, Iervolino I. Spectral shape proxies and nonlinear structural response. *Soil Dynamics and Earthquake Engineering* 2011; **31**(7): 996–1008. DOI: 10.1016/j.soildyn.2011.03.006.
31. Mehanny SSF. A broad-range power-law form scalar-based seismic intensity measure. *Engineering Structures* 2009; **31**(7): 1354–1368. DOI: 10.1016/j.engstruct.2009.02.003.
32. Tsantaki S, Adam C, Ibarra LF. Intensity measures that reduce collapse capacity dispersion of P-delta vulnerable simple systems. *Bulletin of Earthquake Engineering* 2017; **15**(3): 1085–1109. DOI: 10.1007/s10518-016-9994-4.
33. Bazzurro P, Cornell CA. Vector-Valued Probabilistic Seismic Hazard Analysis (VPSHA). *Proceedings of the 7th U.S. National Conference on Earthquake Engineering*, Boston, Massachusetts, USA: 2002.
34. Baker JW, Cornell CA. A vector-valued ground motion intensity measure consisting of spectral acceleration and epsilon. *Earthquake Engineering and Structural Dynamics* 2005; **34**(10): 1193–1217.

DOI: 10.1002/eqe.474.
35. Melissianos VE, Vamvatsikos D, Gantes CJ. Performance Assessment of Buried Pipelines at Fault Crossings. *Earthquake Spectra* 2017; **33**(1): 201–218. DOI: 10.1193/122015EQS187M.
36. Baker JW. Probabilistic structural response assessment using vector-valued intensity measures. *Earthquake Engineering & Structural Dynamics* 2007; **36**(13): 1861–1883. DOI: 10.1002/eqe.700.
37. Gehl P, Seyedi DM, Douglas J. Vector-valued fragility functions for seismic risk evaluation. *Bulletin of Earthquake Engineering* 2013; **11**(2): 365–384. DOI: 10.1007/s10518-012-9402-7.
38. Malhotra PK, Veletsos AS. Uplifting Response of Unanchored Liquid-Storage Tanks. *Journal of Structural Engineering* 1994; **120**(12): 3525–3547. DOI: 10.1061/(ASCE)0733-9445(1994)120:12(3525).
39. CEN. *Eurocode 8: Design of structures for earthquake resistance–Part 4: Silos, tanks and pipelines*. vol. 3. Brussels: 2006.
40. American Petroleum Institute. *Seismic Design of Storage Tanks - Appendix E, Welded Steel Tanks for Oil Storage*. vol. 552. API 650, 11th Edition, Washington, D.C.: 2007.
41. Housner GW. Dynamic pressures on accelerated fluid containers. *Bulletin of the Seismological Society of America* 1957; **47**(1): 15–35.
42. Housner GW. The dynamic behavior of water tanks. *Bulletin of the Seismological Society of America* 1963; **53**(2): 381–387.
43. Vathi M, Karamanos SA. A simple and efficient model for seismic response and low-cycle fatigue assessment of uplifting liquid storage tanks. *Journal of Loss Prevention in the Process Industries* 2017(Article in press). DOI: 10.1016/j.jlp.2017.08.003.
44. Pagani M, Monelli D, Weatherill G, Danciu L, Crowley H, Silva V, *et al.* OpenQuake Engine: An Open Hazard (and Risk) Software for the Global Earthquake Model. *Seismological Research Letters* 2014; **85**(3): 692–702. DOI: 10.1785/0220130087.
45. Giardini D, Woessner J, Danciu L, Crowley H, Cotton F, Grünthal G, *et al.* Seismic Hazard Harmonization in Europe (SHARE): Online Data Resource 2013. DOI: 10.12686/SED-00000001-SHARE.
46. Boore DM, Atkinson GM. Ground-Motion Prediction Equations for the Average Horizontal Component of PGA, PGV, and 5%-Damped PSA at Spectral Periods between 0.01 s and 10.0 s. *Earthquake Spectra* 2008; **24**(1): 99–138. DOI: 10.1193/1.2830434.
47. Kohrangi M, Bazzurro P, Vamvatsikos D. Vector and Scalar IMs in Structural Response Estimation, Part I: Hazard Analysis. *Earthquake Spectra* 2016; **32**(3): 1507–1524. DOI: 10.1193/053115EQS080M.
48. Ancheta T, Darragh R, Stewart J, Seyhan E, Silva W, Chiou B, *et al. PEER NGA-West2 Database, Technical Report PEER 2013/03*. Pacific Earthquake Engineering Research Center, Berkeley, CA: 2013.
49. Lin T, Haselton CB, Baker JW. Conditional spectrum-based ground motion selection. Part I: Hazard consistency for risk-based assessments. *Earthquake Engineering & Structural Dynamics* 2013; **42**(12): 1847–1865. DOI: 10.1002/eqe.2301.
50. Kohrangi M, Bazzurro P, Vamvatsikos D, Spillatura A. Conditional spectrum-based ground motion record selection using average spectral acceleration. *Earthquake Engineering & Structural Dynamics* 2017; **44**: 657–675. DOI: 10.1002/eqe.2876.
51. Jayaram N, Lin T, Baker JW. A Computationally Efficient Ground-Motion Selection Algorithm for Matching a Target Response Spectrum Mean and Variance. *Earthquake Spectra* 2011; **27**(3): 797–815. DOI: 10.1193/1.3608002.
52. Kohrangi M, Vamvatsikos D, Bazzurro P. Conditional spectrum based record selection at multiple IM levels for IDA (under review).
53. Kohrangi M, Bazzurro P, Vamvatsikos D. Implementing Conditional Spectrum based record selection for nonlinear dynamic analysis of 3D structural models: an introduction to vector IM based conditional spectra (under review).
54. Kishida T. Conditional Mean Spectra Given a Vector of Spectral Accelerations at Multiple Periods. *Earthquake Spectra* 2017; **33**(2): 469–479. DOI: 10.1193/052316EQS086EP.
55. Nuzzo R. Scientific method: Statistical errors. *Nature* 2014; **506**(7487): 150–152. DOI: 10.1038/506150a.
56. Jalayer F, Beck JL, Zareian F. Analyzing the Sufficiency of Alternative Scalar and Vector Intensity Measures of Ground Shaking Based on Information Theory. *Journal of Engineering Mechanics* 2012; **138**(3): 307–316. DOI: 10.1061/(ASCE)EM.1943-7889.0000327.

57. Ebrahimian H, Jalayer F, Lucchini A, Mollaioli F, Manfredi G. Preliminary ranking of alternative scalar and vector intensity measures of ground shaking. *Bulletin of Earthquake Engineering* 2015; **13**(10): 2805–2840. DOI: 10.1007/s10518-015-9755-9.
58. Inoue T. Seismic Hazard Analysis of Multi-Degree-Of-Freedom Structures. Reliability of Marine Structures, RMS-8, Stanford, California, 1990.
59. Baker JW, Cornell CA. Correlation of response spectral values for multicomponent ground motions. *Bulletin of the Seismological Society of America* 2006; **96**(1): 215–227. DOI: 10.1785/0120050060.

